

Kramers-Kronig Constrained Modeling of Soft X-ray Reflectivity Spectra - Obtaining Depth Resolution of Electronic and Chemical Structure

Kevin H. Stone* and Jeffrey B. Kortright†

Materials Sciences Division, Lawrence Berkeley National Lab, Berkeley, CA 94720

S. Manuel Valvidares

ALBA Synchrotron Light Source, 082980 Cerdonyola del Vallès, Barcelona, Spain

(Dated: April 27, 2012)

Abstract

Resonant x-ray scattering is a powerful technique for the determination of electronic structure at the nanoscale. In common practice, the optical properties of the constituent components of a material must be known prior to modeling of the scattered intensity. We present a means of refining electronic structure, in the form of optical properties, simultaneous to physical structure, in a Kramers-Kronig consistent manner. This approach constitutes a sensitive and powerful extension of resonant x-ray scattering to materials where the optical properties are not sufficiently well known. The application of this approach to specular reflectivity from a single crystal of SrTiO₃ is presented as an example case, wherein we find evidence for both a non-resonant surface contaminant layer and a modified SrTiO₃ surface region. Extrapolating from this study we comment on the potential utility of this approach to resonant scattering studies in general.

DISCLAIMER

This document was prepared as an account of work sponsored by the United States Government. While this document is believed to contain correct information, neither the United States Government nor any agency thereof, nor the Regents of the University of California, nor any of their employees, makes any warranty, express or implied, or assumes any legal responsibility for the accuracy, completeness, or usefulness of any information, apparatus, product, or process disclosed, or represents that its use would not infringe privately owned rights. Reference herein to any specific commercial product, process, or service by its trade name, trademark, manufacturer, or otherwise, does not necessarily constitute or imply its endorsement, recommendation, or favoring by the United States Government or any agency thereof, or the Regents of the University of California. The views and opinions of authors expressed herein do not necessarily state or reflect those of the United States Government or any agency thereof or the Regents of the University of California.

I. INTRODUCTION

Resonant x-ray scattering extends anomalous scattering¹ across atomic core levels to combine the element and state specific electronic structure available from absorption measurements with information on spatial correlations available from angle resolved scattering. Such an approach can elucidate aspects of the spatial distribution of electronic or chemical structure not available away from resonance²⁻⁷. It constitutes a growing application of tunable synchrotron radiation and promises access to ultrafast electron dynamics at short length scales in x-ray free-electron laser sources. Strong, sharp absorption features at the soft x-ray core levels makes resonant x-ray scattering an attractive tool to study important aspects in magnetic, correlated electron, and even polymeric systems with nanometer-scale resolution and greater penetrating power than powerful electron spectroscopies.

In the near-visible spectral region several methods are widely used to obtain absolute optical constants, including their spectral and depth dependence, from reflectance data⁸⁻¹⁰. Such methods include reflectometry, ellipsometry, and polarimetry, and generally aim to determine the real and imaginary parts of a complex index of refraction through measurements of reflected intensity, phase change, and/or polarization. At discrete photon energies,

modeling angle-resolved data is common and may or may not yield results consistent with the Kramers-Kronig (KK) dispersion relation. Full spectroscopic determinations require energy-resolved measurements and their analysis in a manner ensuring KK consistency. The same approaches and challenges apply in the soft x-ray range, although here it is much easier to measure scattered intensity than polarization or phase.

Resonant x-ray scattering intensities are generally described as the modulus squared of a complex optical contrast involving one or more complex refractive indices, $n = 1 - \delta - i\beta$. Applications often require accurate resonant x-ray absorption spectra (commonly referred to as XAS, NEXAFS, or XANES) to interpret results. Such spectra are obtained either from measurement or some form of model calculation, and are often adequate for the problem at hand^{11,12}. However, as resonant x-ray scattering applications become more refined, cases are encountered in which the spatial distribution of electronic structure itself is to be determined, and in such cases it is not obvious that measured or model optical spectra are sufficient. Rather, obtaining the spatial distribution of resonant optical properties directly by simultaneously modeling spectroscopy and structure in fitting experimental data would provide a useful alternative. Fixed-energy determinations of optical constants are common in the x-ray region (generally through fitting of angular resolved reflectivity, $R(Q)$)¹³⁻²¹. While this approach has been extended to fitting fixed energy reflectivity data at a number of energies spanning the atomic core level as a means of spectroscopy²², full spectroscopic analysis is not generally applied to reflectivity data.

Here we present a flexible approach to model spectra and structure on equal footing in fitting reflected intensities, using a variational algorithm²³ to efficiently ensure KK consistency between δ and β as they refine along with structural parameters to yield a self-consistent model of the spatial distribution of electronic structure. This variational approach is designed to model spectra of arbitrary shape to provide accurate absolute values for optical spectra within the assumptions of the structural model, which may also be refined in the modeling process. This is an extension of an earlier approach to reflectivity modeling that used a small number of Lorentzian peaks to describe the absorption spectra²⁴. The current approach is similar, but allows for much greater flexibility to fit the fine details of a measured reflectivity spectrum.

To illustrate this approach we apply it to determine the resonant optical properties across the Ti $L_{2,3}$ and O K edges in a single crystal of SrTiO₃ (001) (STO). This material was

chosen because STO remains technologically important and because its near surface region is known to exhibit subtle and complex behavior which remains a topic of active study²⁴⁻²⁷. We find evidence that two surface layers, a contamination layer atop an STO-like layer departing from bulk properties, are needed to explain the specific set of experimental data that we model. Below, the variational approach and fitting strategy are described, followed by its systematic application to reflected intensity spectra measured at several fixed incidence angles. Comments on its potential utility are given in the conclusion.

II. REFLECTIVITY MODELING

Our goal is to measure specular reflectivity as a function of x-ray energy across the resonant absorption edges of a material and then fit this with a model of both physical and electronic structure. The electronic structure is, for our purposes, that projected by resonant dipole transitions onto the optical properties as represented by the complex refractive index, $n = 1 - \delta - i\beta$. The real and imaginary parts of the index of refraction are directly related to the complex atomic scattering factors, $f(h\nu) = f_0 - f'(h\nu) - if''(h\nu)$, through

$$n(h\nu) = 1 - \delta(h\nu) - i\beta(h\nu) = 1 - \frac{r_e c^2 N_A}{2\pi\nu^2} \sum_i \frac{Z_i}{A_i} \rho_i f_i(h\nu), \quad (1)$$

where r_e is the classical electron radius, ρ_i is the density due to atom i such that $\sum \rho_i = \rho$, N_A is Avogadro's number, Z_i and A_i are the atomic number and weight of atom i , respectively, and $f_0 = Z - (\frac{Z}{82.5})^{2.37}$. We wish to determine the values of $f_i(h\nu)$ which give the best agreement to the measured reflectivity. The KK relation allows us to determine the real part of the atomic scattering factor from the imaginary part, or *vice versa*. We work with the imaginary part of the atomic scattering factor, as its features are generally well localized and necessarily positive, as opposed to the dispersive nature of the real part, which may also change sign near resonance. The relevant KK relation is then given by

$$f'(h\nu) = \frac{2}{\pi} \oint_0^\infty \frac{h\nu'}{(h\nu)^2 - (h\nu')^2} f''(h\nu') dh\nu'. \quad (2)$$

Having measured the reflectivity at a discrete set of energies $\{h\nu_j\}$, it is natural to then determine f'' at these same energies. We use the KK relation to obtain f' at these discrete energies to calculate the reflectivity for comparison with measurement. Unfortunately, the

formula for specular reflectivity cannot, in general, be inverted to directly solve for the atomic scattering factors, so we must resort to iterative methods to solve for the values of f'' . Thus repeated KK transformations are required. This can be efficiently achieved using KK consistent functions to represent f'' and f' , such as symmetrized Lorentzians or Gaussians for absorption lines²⁸ as we recently demonstrated for resonant reflectivity²⁴. However arbitrary f'' shapes are not generally compatible with the extended tails of Lorentzian absorption lines. Here we implement a much more flexible and general approach to avoid repeated KK evaluations, namely the variational approach of Kuzmenko²³.

A. The Variational Approach

In the variational approach, we write f'' as a sum of basis functions

$$f''(h\nu) = \sum_j C_j f_j^{basis}(h\nu). \quad (3)$$

In this way, we can uniquely define an arbitrary spectral shape through the set of coefficients C_j and the appropriate basis function. We assume the shape of f'' to be smooth within the resolution of our measurement. To ensure that our refined spectra has this feature, we select a basis function that includes point to point correlations. Namely, we choose a triangle function that extends to the next nearest neighbor, see Figure 1,

$$f_j^{basis}(h\nu) = \Delta_j(h\nu) = \begin{cases} \frac{(h\nu - h\nu_{j-2})}{(h\nu_j - h\nu_{j-2})} & h\nu_{j-2} < h\nu < h\nu_j \\ \frac{(h\nu_{j+2} - h\nu)}{(h\nu_{j+2} - h\nu_j)} & h\nu_j < h\nu < h\nu_{j+2} \\ 0 & \text{otherwise} \end{cases} \quad (4)$$

Thus each point will depend on its nearest neighbors,

$$f''(h\nu_j) = C_{j-1} \Delta_{j-1}(h\nu_j) + C_j \Delta_j(h\nu_j) + C_{j+1} \Delta_{j+1}(h\nu_j), \quad (5)$$

so that there is an inherent point to point correlation in any result, ensuring local smoothness. While we have chosen this particular basis function for its convenience, there are many others that would also be suitable, as detailed more thoroughly in the work by Kuzmenko²³. However, this ensemble of triangle functions allows for a locally smooth, continuous result from a large number of nearly independent parameters, avoiding the issue of overlap that would arise from any function with extended tails, such as Gaussian or Lorentzian functions.

The primary benefit to expressing f'' in this manner is that we can write an analytical expression for the KK transform of our basis function,

$$KK[\Delta_j(h\nu)] = \frac{1}{\pi} \left[\frac{g(h\nu, h\nu_{j-2})}{h\nu_j - h\nu_{j-2}} - \frac{(h\nu_{j+2} - h\nu_{j-2})g(h\nu, h\nu_j)}{(h\nu_j - h\nu_{j-2})(h\nu_{j+2} - h\nu_j)} + \frac{g(h\nu, h\nu_{j+2})}{h\nu_{j+2} - h\nu_j} \right] \quad (6)$$

with

$$g(x, y) \equiv (x + y) \ln |x + y| + (x - y) \ln |x - y| \quad (7)$$

which allows us to write f' as the linear combination

$$f'(h\nu) = \sum_j C_j KK\{\Delta_j(h\nu)\}. \quad (8)$$

Evidently, as both $f'(h\nu)$ and $f''(h\nu)$ depend on the same set of coefficients C_j , changing a single point in $f''(h\nu)$ does not require the full KK transformation to update $f'(h\nu)$, instead a single term of the above sum is simply adjusted to update the previous spectrum and maintain KK consistency. This variational approach greatly reduces the computational burden while maximizing the flexibility to represent arbitrary spectral shapes.

B. Maximum Entropy

One drawback to the variational approach to modeling reflectivity data is the large number of free parameters needed to define a spectral and physical model. Parameterizing the absorption spectra at each measured x-ray energy implies a roughly equal number of refinable parameters as data points, making the problem underconstrained. As a result, we cannot be certain to refine towards a stable solution representing the global minimum, nor that any such solution will be unique. We find a solution to this problem in the field of information theory, namely the principle of maximum entropy²⁹. We define an entropy as

$$S = \sum_j C_j - m_j - C_j \ln \frac{C_j}{m_j} \quad (9)$$

where m_j are the default values for our parameters and represent the solution we would prefer in the absence of any data, which for practical purposes is our set of starting values. We consider the entropy as a constraint in our fit to the data which helps to stabilize the least-squares fitting for a free-form solution. Instead of considering just the set of parameters which give the best fit to the measured data, we will search for the set of parameters that

give sufficient agreement with the data and simultaneously maximize the entropy. This can be accomplished through the use of a Lagrange multiplier, λ , in maximizing

$$\lambda S - \frac{\chi^2}{2}, \quad (10)$$

where χ^2 represents the least-squares metric, or other appropriate figure of merit.

The maximum entropy solution is unique, and will deviate as little as necessary from the starting model while still fitting the data. While there are many ways of solving the maximum entropy equation (10)³⁰⁻³², they will all, in general, maintain positivity for the refined parameters. As all of the parameters should be positive (representing things such as layer thickness, roughness, density, composition, or absorption, all of which may be refined³³), this is an advantageous feature which helps to ensure a physically meaningful result.

III. THE SrTiO₃ (001) SURFACE - AN EXAMPLE CASE

As an example of the method, we consider the Ti *L*-edge and O *K*-edge of a SrTiO₃ (100) single crystal measured using specular reflectivity data, $R(h\nu)$, at several discrete incidence angles, θ . SrTiO₃ (STO) is a common substrate for thin film growth and an important dielectric material in its own right. STO represents an interesting test case which has been well studied and is suitably complex so as not to be trivial. In fact, the large number of studies on the STO surface are not all in agreement, possibly due to the dynamic nature of the surface. While this makes comparison of our results to those in the literature difficult, it also presents an opportunity for a unique look at this complex system.

The data presented here were measured on a commercially obtained (100) oriented substrate roughly 5mm square, treated with HF to ensure a Ti terminated surface. Prior to these measurements, this sample had been exposed to vacuum and x-rays in earlier measurements, and stored for extended periods in atmosphere. Data were collected at Beamline 6.3.2 of the Advanced Light Source at Lawrence Berkeley National Laboratory at incidence angles of 14°, 15°, 16°, 17°, and 30° in a single session and are considered internally self-consistent. Care was taken to correctly normalize all reflectivity spectra to the incident beam spectrum in order to obtain the best values for the absolute reflectivity. Refinements were done using our reflectivity analysis program written in Python. The program uses the

variational approach and maximum entropy to refine f'' values of resonant atoms and physical parameters of the model for the sample. Reflectivities are calculated using the Parratt formalism³⁴ with the inclusion of a Névo-Croce³⁵ roughness correction for each interface. Refinement details for each model considered can be found in Table I.

To start, we consider the simplest possible model, that of a semi-infinite slab of stoichiometric STO (model #1). In order to simplify and speed up the refinement procedure, we begin by considering only the data measured over the Ti edge at a incidence angle of $\theta = 15^\circ$. The refinement starts from a four Lorentzian model spectra for the Ti edge, similar to that used by Valvidares *et al*²⁴. The results are shown in Figure 2. The fit to the measured reflectivity is essentially perfect, indicating that the refinement has proceeded as intended. However, even a cursory inspection of the resulting f'' spectra shows serious deficiencies. The dotted line is the tabulated Henke data³⁶ showing the continuum step, and the solid line is the result of the refinement. A physically meaningful absorption spectra should approach the tabulated values away from resonance, and have a sharp onset of resonant features near the continuum step in the tabulated data. The refined spectra has two obvious problems, it rises significantly at energies well below the onset of resonance, and it dips slightly below the pre-edge values at energies above resonance ($\sim 468\text{eV}$). Both of these features are unphysical, indicating that this structural model is incorrect in some way.

As a modification to the naïve model #1, we include the possibility of a non-resonant surface layer, which we assume to be composed of carbonaceous material (model #2). This is the simplest modification of model #1 and represents the likely possibility that the sample surface is not perfectly clean. We fit model #2 to a larger subset of the available data, that at $\theta = 14^\circ, 15^\circ, 16^\circ$, and 17° over both the Ti and O edges. Note that this approach deals naturally with compound edges where absorption features of different atoms may overlap. We refine the thickness, density, and surface roughness of the non-resonant surface layer, the interfacial roughness, and the f'' spectra for Ti and O in the STO layer. We limit the refinable range for the absorption spectra to be between 440eV and 500eV for Ti and between 525eV and 600eV for O. The starting point for this model will be the result of the Lorentzian modeling for the Ti spectra and the absorption measured from total electron yield for the O edge measured concomitantly with the $\theta = 15^\circ$ reflectivity with a 5Å thick carbon top layer and all roughnesses being equal to 2Å. The results of model #2 are shown in Figure 3.

Model #2 represents a significant improvement from the result of model #1. The fit to all of the refined data is good, though not perfect, but more importantly, the resulting f'' spectra does not show the same severe unphysical behavior as in model #1. Examination of the physical structure shows plausible parameters as well (Table I). However, closer inspection of the reflectivity fits, especially at the Ti edge, shows a systematic variation as we move up in angle such that the model progresses towards an underestimation of the data on resonance, and an overestimation away from resonance. This systematic trend is extremely pronounced at $\theta = 30^\circ$, indicating again that structural model #2 is oversimplified. Understanding the nature of Keissig (thickness) fringes whereby interference minima move from high Q toward low Q as layer thickness increases, the strong θ dependence of fit quality suggests the presence of a thicker layer in addition to the thin carbonaceous layer.

Clearly, the inclusion of a non-resonant surface layer is important, but not sufficient to explain our data. It is also clear that we benefit from the inclusion of as much data as possible in our model refinements, and so will refine our models against all available data henceforth. As a further modification of our STO model, we refer to the literature on this material, which suggests that there may exist a distinct surface region within the STO itself²⁴⁻²⁷. This surface region may have a composition distinct from the bulk STO and/or may exhibit different spectral features for the resonant atoms. This suggests two possible models, one with distinct composition between the two STO regions, but common spectra for the resonant atoms (model #3a), and one with both distinct composition and spectra (model #3b)³⁷. We consider the simpler of these, model #3a, first.

The thickness of the resonant STO surface region is initially assumed to be 20Å, in accord with recent results from Valvidares *et al*²⁴. We make the starting point of the refinement of model #3a the endpoint of model #2 by giving the resonant surface region the same composition as that of the bulk, and setting the spectra for both to the refined result of model #2. In the interest of charge balance, we constrain the composition of the surface region in our model to be a mixture of SrO and TiO₂. This is a much simpler calculation than for model #3b while still allowing for a distinct STO-like surface region to exist, the results of which can be seen in Figure 4.

Model #3a is a significant improvement upon model #2. The reflectivities are all well fit, and the resulting spectra for the Ti and O edges show no unphysical behavior. There is still a small systematic discrepancy between measured and calculated reflectivity near the

Ti edge, and some misfitting of the O edge in the $\theta = 30^\circ$ data, although that may be due to higher levels of noise in the data at that angle. All in all, this is a good model, and might well be considered sufficient for this set of data.

In the spirit of completeness, and to explore the limits of this technique, we consider model #3b, with distinct Ti and O spectra for the surface and bulk regions of the STO. The starting point for this refinement will be the result of the refinement for model #3a, and we let the surface and bulk STO spectra refine away from this point. The results of the refinement for model #3b are shown in Figure 5.

The improvement beyond model #3a is subtle, and best seen in the decrease in the figure of merit by roughly 35%. Given that the number of parameters being fit has nearly doubled, it is unclear just how significant this improvement is. It is also clear that the differences in spectra between the resonant surface region and the bulk STO are subtle at best. Presumably questions as to the significance of these differences could be addressed with a more complete data set, including $R(h\nu)$ at a larger set of incidence angles as well as $R(Q)$ at discrete $h\nu$. While this method is capable of refining multiple spectra, even for the same element, it seems apparent that the distinct surface region in STO exhibits little spectral variation from the bulk, and is instead due primarily to compositional changes. As such it seems unnecessary to consider models of any greater complexity.

IV. DISCUSSION AND CONCLUSIONS

Variational fitting of reflectivity spectra is a powerful approach for extracting resonant optical constants for a material. We have taken as an example the case of a bare STO substrate. We find evidence for both a resonant STO-like surface region as well as a non-resonant contamination layer above that. The resonant surface region exhibits only subtle spectroscopic variation from the bulk, but does have a distinct composition with an enhanced SrO:TiO₂ ratio which provides optical contrast. This result is not in complete agreement with a previous study on the same material using the less sensitive Lorentzian lineshape approach²⁴ which found evidence for a resonant surface region, but did not consider the possibility of a non-resonant contamination layer. This may be due to the complex and dynamic nature of the STO surface, such that the samples measured may not exhibit the same surface behavior. It is also possible that the nature of the STO-like surface region ap-

pears differently when the model is constrained by a Lorentzian lineshape in the absence of a non-resonant surface layer, as in that earlier work. Such constraints allow for a reasonable overall fit, but give poor agreement in the fine details of the measured spectra. The variational algorithm models this fine detail, which may possess much of the critical information about a sample.

This example illustrates some of the more important considerations in modeling of resonant reflectivity data. While an initial starting spectra is necessary, no specific assumptions about the details of the resonant spectra at a given edge need to be made for the method to converge. An optical spectra will generally result, even if the structural model is inadequate, and in such cases the result must be considered as an *effective* optical spectra within the context of a given model, such as for model #1 above.

It is thus essential to have criteria available to judge whether a given refined spectral-structural model is acceptable. Such criteria can include physical constraints on the resultant absorption spectra, which should be positive with proper limiting behavior in the pre- and post-edge regions. Systematic effects tend to occur near resonance due to overlayers and can be useful as a guide towards a more suitable model. Results should also be consistent with information from other measurements, and self-consistent within the largest dataset available, including spectra measured at various incidence angles and angle resolved data. The uniqueness and accuracy of the final spectra ultimately relies on the self-consistency between the structural and spectral aspects of a model. Spectral self-consistency derives from explicit inclusion of KK consistency, and structural self-consistency will derive from modeling spectral behavior at many angles, as done here, or through the explicit inclusion of angle dependent scans at one or more energies. Provided that self-consistency is reached, the optical spectra can be considered as absolute and free from measurement artifacts that plague many soft x-ray spectroscopies.

The approach presented here may be readily extended to any form of resonant scattering, not just specular reflectivity, provided a suitable expression for the scattering intensity is available for refinement. Reflectivity from stratified systems represents an obvious and broad class of problems amenable to this analysis, as demonstrated here. This approach of fitting reflectivity data, or indeed any resonant scattering data, solves a number of outstanding problems in spectroscopy. The technique deals quite naturally with overlapping edges, as demonstrated here by the weakly overlapping Ti and O spectra. Spatial inhomogeneities

are commonly averaged in soft x-ray spectroscopy, whereas this approach relies on them and determines the spatial distribution of their spectral composition as a matter of course. Scattered intensities are generally easy to measure, making this approach less susceptible to measurement artifacts such as saturation effects in electron yield, or self-absorption in fluorescence yield experiments, while being applicable to a wide variety of sample geometries. Most importantly, this approach ensures a self consistent description of spectroscopic and structural aspects of the sample.

The computational burden required to converge to acceptable tolerances is determined by the complexity of the structural model, both in the number of layers and the number of parameters, and the amount of data being fit. The method is designed to be very efficient in this respect and can be scaled up to problems of arbitrary size and complexity. To this end, advances in computing power and developments in highly parallel processing will clearly be of interest to this approach in the future.

ACKNOWLEDGMENTS

Research, including measurements using beamlines 4.0.2, 8.0.1, and 6.3.2 at the Advanced Light Source (LBNL), was supported by the U.S. Department of Energy, Office of Basic Energy Sciences, Division of Materials Sciences and Engineering under Contract No. DE-AC02-05CH11231. A U.S. Spain Fulbright supported S.M.V. for part of this work.

* kstone@lbl.gov

† jbkortright@lbl.gov

¹ Anomalous x-ray scattering typically refers to changes in the real part of atomic scattering factors as $h\nu$ is tuned below the absorption edge.

² H. A. Dürr, E. Dudzik, S. S. Dhesi, J. B. Goedkoop, G. van der Laan, M. Belakhovsky, C. Mocuta, A. Marty, and Y. Samson, *Science* **284**, 2166 (1999).

³ J. B. Kortright, S.-K. Kim, G. P. Denbeaux, G. Zeltzer, K. Takano, and E. E. Fullerton, *Phys. Rev. B* **64**, 092401 (2001).

- ⁴ P. Abbamonte, L. Venema, A. Rusydi, G. A. Sawatzky, G. Logvenov, and I. Bozovic, *Science* **297**, 581 (2002).
- ⁵ S. B. Wilkins, P. D. Hatton, M. D. Roper, D. Prabhakaran, and A. T. Boothroyd, *Phys. Rev. Lett.* **90**, 187201 (2003).
- ⁶ K. J. Thomas, J. P. Hill, S. Grenier, Y.-J. Kim, P. Abbamonte, L. Venema, A. Rusydi, Y. Tomioka, Y. Tokura, D. F. McMorrow, G. Sawatzky, and M. van Veenendaal, *Phys. Rev. Lett.* **92**, 237204 (2004).
- ⁷ S. Roy, M. R. Fitzsimmons, S. Park, M. Dorn, O. Petravic, I. V. Roshchin, Z.-P. Li, X. Batlle, R. Morales, A. Misra, X. Zhang, K. Chesnel, J. B. Kortright, S. K. Sinha, and I. K. Schuller, *Phys. Rev. Lett.* **95**, 047201 (2005).
- ⁸ R. M. A. Azzam and N. M. Bashara, *Ellipsometry and Polarized Light* (North-Holland Amsterdam, 1977).
- ⁹ E. D. Palik, *Handbook of Optical Constants of Solids* (Academic Press, Inc., 1985).
- ¹⁰ H. G. Tompkins and W. A. McGahan, *Spectroscopic Ellipsometry and Reflectometry; A Users Guide* (John Wiley and Sons, 1999).
- ¹¹ S. D. Brown, L. Bouchenoire, P. Thompson, R. Springell, A. Mirone, W. G. Stirling, A. Beesley, M. F. Thomas, R. C. C. Ward, M. R. Wells, S. Langridge, S. W. Zochowski, and G. H. Lander, *Phys. Rev. B* **77**, 014427 (2008).
- ¹² L. Bouchenoire, A. Mirone, S. D. Brown, P. Strange, T. Wood, P. Thompson, D. Fort, and J. Fernández-Rodríguez, *New J. Phys.* **11**, 123011 (2009).
- ¹³ J. M. Tonnerre, L. Seve, D. Raoux, G. Soullie, B. Rodmacq, and P. Wolfers, *Phys. Rev. Lett.* **75**, 740 (1995).
- ¹⁴ M. Wormington, C. Panaccione, K. Matney, and D. Bowen, *Philos. Trans. R. Soc. London, Ser. A* **357**, 2827 (1999).
- ¹⁵ M. Sacchi, C. F. Hague, E. M. Gullikson, and J. H. Underwood, *Phys. Rev. B* **57**, 108 (1998).
- ¹⁶ I. Diel, J. Friedrich, C. Kunz, S. DiFornzo, B. R. Muller, and W. Jark, *Appl. Opt.* **36**, 6376 (1997).
- ¹⁷ J. E. Prieto, F. Heigl, O. Krupin, G. Kaindl, and K. Starke, *Phys. Rev. B* **68**, 134453 (2003).
- ¹⁸ A. van der Lee, F. Salah, and B. Harzallah, *J. Appl. Cryst.* **40**, 820 (2007).
- ¹⁹ S. M. Danauskas, D. Li, M. Meron, B. Lin, and K. Y. C. Lee, *J. Appl. Cryst.* **41**, 1187 (2008).

- ²⁰ R. Soufli, A. L. Aquila, F. Salmassi, M. Fernandez-Perea, and E. M. Gullikson, *Appl. Opt.* **47**, 4633 (2008).
- ²¹ M. Mezger, B. Jerome, J. B. Kortright, M. Valvidares, E. M. Gullikson, A. Giglia, N. Mahne, and S. Nannarone, *Phys. Rev. B* **83**, 155406 (2011).
- ²² D. Ksenzov, T. Panzner, C. Schlemper, C. Morawe, and U. Pietsch, *Appl. Opt.* **48**, 6684 (2009).
- ²³ A. B. Kuzmenko, *Review of Scientific Instruments* **76**, 083108 (2005).
- ²⁴ S. M. Valvidares, M. Huijben, P. Yu, R. Ramesh, and J. B. Kortright, *Phys. Rev. B* **82**, 235410 (2010).
- ²⁵ W. Meevasana, P. D. C. King, R. H. He, S. K. Mo, M. Hashimoto, A. Tamai, P. Songsiriritthigul, F. Baumberger, and Z. X. Shen, *Nature Mater.* **10**, 114 (2011).
- ²⁶ A. F. Santander-Syro, O. Copie, T. Kondo, F. Fortuna, S. Pailhes, R. Weht, X. G. Qiu, F. Bertran, A. Niolaou, A. Taleb-Ibrahimi, P. L. Fevre, G. Herranz, M. Bibes, N. Reyren, Y. Apertet, P. Lecoeur, A. Barthelemy, and M. J. Rozenberg, *Nature* **469**, 189 (2011).
- ²⁷ K. Szot and W. Speier, *Phys. Rev. B* **60**, 5909 (1999).
- ²⁸ C. D. Keefe, *J. Mol. Spectrosc.* **205**, 261 (2001).
- ²⁹ D. S. Sivia and J. Skilling, *Data Analysis a Bayesian Tutorial* (Oxford University Press, 2007).
- ³⁰ S. F. Gull and G. J. Daniell, *Nature* **272**, 686 (1978).
- ³¹ J. Skilling and R. K. Bryan, *Mon. Not. R. ast. Soc.* **211**, 111 (1984).
- ³² M. Sakata and M. Sato, *Acta. Cryst.* **A46**, 263 (1990).
- ³³ We have implemented this algorithm in a Python script, which can be made available upon request. The program is capable of implementing a number of algorithms for solving the maximum entropy equation (or performing a minimization without entropy considerations), as well as using a number of possible forms for the figure of merit. We generally prefer a modification of the algorithm developed by Gull and Daniell with a figure of merit of the form $\left(\frac{Y_{\text{obs}} - Y_{\text{calc}}}{Y_{\text{obs}}}\right)^2$.
- ³⁴ L. G. Parratt, *Phy. Rev.* **95**, 359 (1954).
- ³⁵ Névot, L. and Croce, P., *Rev. Phys. Appl. (Paris)* **15**, 761 (1980).
- ³⁶ B. Henke, E. Gullikson, and J. Davis, *Atomic Data and Nuclear Data Tables* **54**, 181 (1993).
- ³⁷ In models #3a and #3b the non-resonant surface layer is still present. We considered models with a resonant surface region in the absence of this non-resonant contamination layer, but found them to give poor fits. It was also noted that the refined spectra for the surface region contained very little resonant character, suggesting a preference for a non-resonant surface layer.

FIG. 1. (Color Online) A gaussian function (dashed line), sampled at discrete points (circles), and approximated by a sum of basis triangle functions (grey), leading to a linear approximation to the original function (blue). The KK transform of a single triangle function (green) as well as the sum of all such functions representing the KK transform of the full gaussian function (red) are also shown.

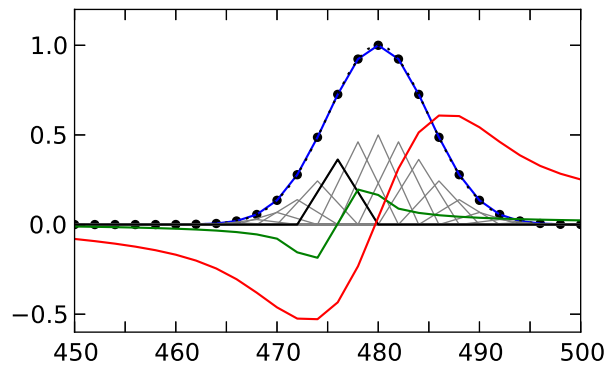


FIG. 2. (Color Online) Results of refinement of model #1. Reflectivity, (a), across the Ti $L_{2,3}$ edge measured at $\theta = 14^\circ$ (black circles) and calculated from the refined model (red line). The resulting spectrum for the imaginary part of the atomic scattering factor, f'' , (solid line) is shown in (b), along with the step function from the tabulated data (dotted line) for that edge for comparison. Only the data shown was considered for the refinement of this model.

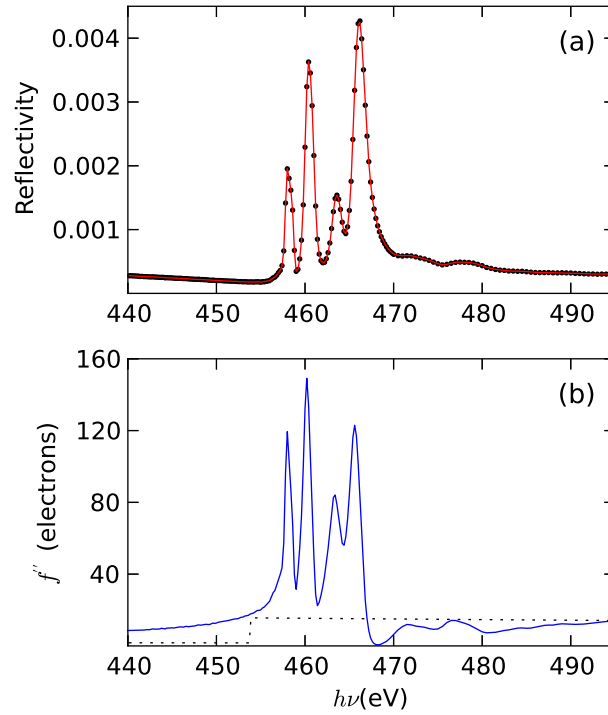


FIG. 3. (Color Online) Results of refinement of model #2. Reflectivity, (a), across the Ti $L_{2,3}$ and O K edges measured at $\theta = 14^\circ, 15^\circ, 16^\circ, 17^\circ$, and 30° (black circles) and calculated from the refined model (red line) are shown top to bottom. The Ti $L_{2,3}$ edge is shown in finer detail in (b), showing the systematic trend towards underfitting of the data at higher angle. Note that the reflectivity at $\theta = 30^\circ$ is shown here, but was not considered in the refinement of this model. The resulting spectra for the imaginary part of the atomic scattering factors, f'' , are shown in (b) for Ti and (c) for O, along with the step functions from the tabulated data for that edge for comparison.

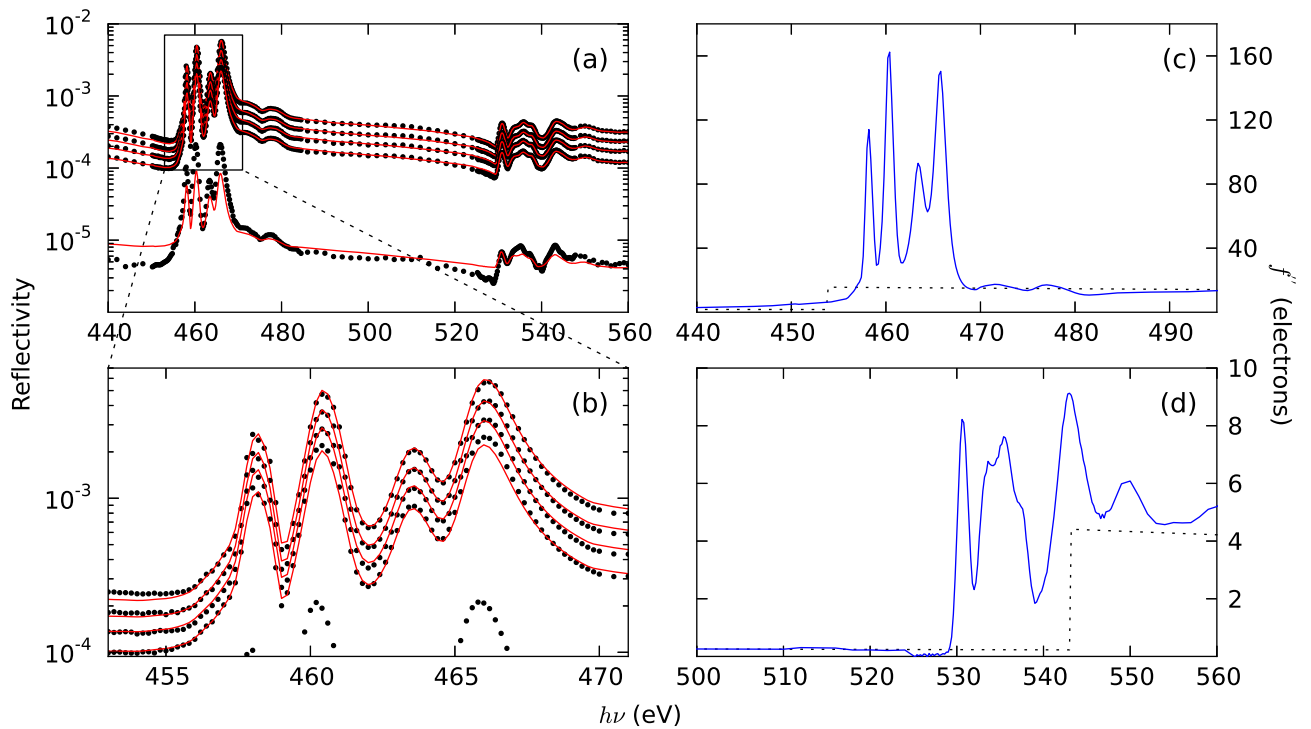


FIG. 4. (Color Online) Results of refinement of model #3a. Reflectivity, (a), across the Ti $L_{2,3}$ and O K edges measured at $\theta = 14^\circ, 15^\circ, 16^\circ, 17^\circ,$ and 30° (black circles) and calculated from the refined model (red line) are shown top to bottom. The Ti $L_{2,3}$ edge is shown in finer detail in (b). All data shown were considered in the refinement of this model. The resulting spectra for the imaginary part of the atomic scattering factors, f'' , are shown in (b) for Ti and (c) for O, along with the step functions from the tabulated data for that edge for comparison.

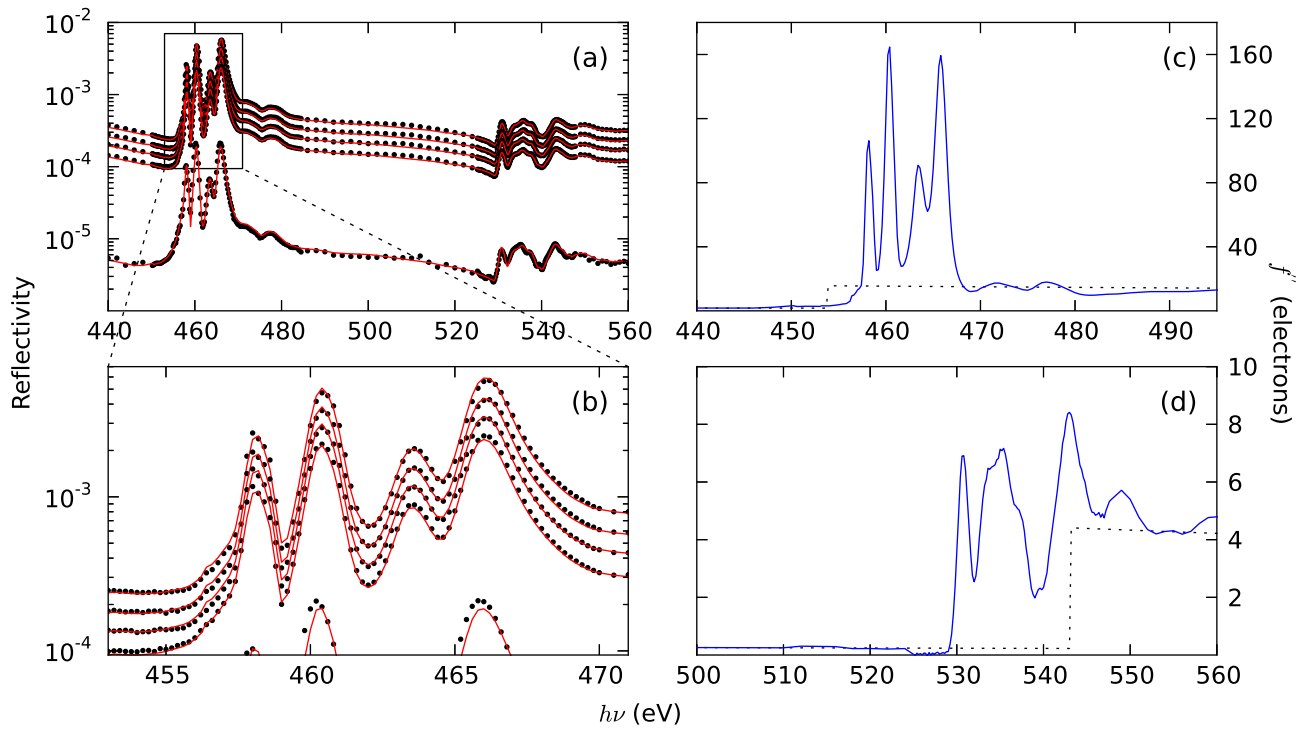


FIG. 5. (Color Online) Results of refinement of model #3b. Reflectivity, (a), across the Ti $L_{2,3}$ and O K edges measured at $\theta = 14^\circ, 15^\circ, 16^\circ, 17^\circ,$ and 30° (black circles) and calculated from the refined model (red line) are shown top to bottom. The Ti $L_{2,3}$ edge is shown in finer detail in (b). All data shown were considered in the refinement of this model. The resulting spectra for the imaginary part of the atomic scattering factors, f'' , are shown in (b) for Ti and (c) for O, along with the step functions from the tabulated data for that edge for comparison.

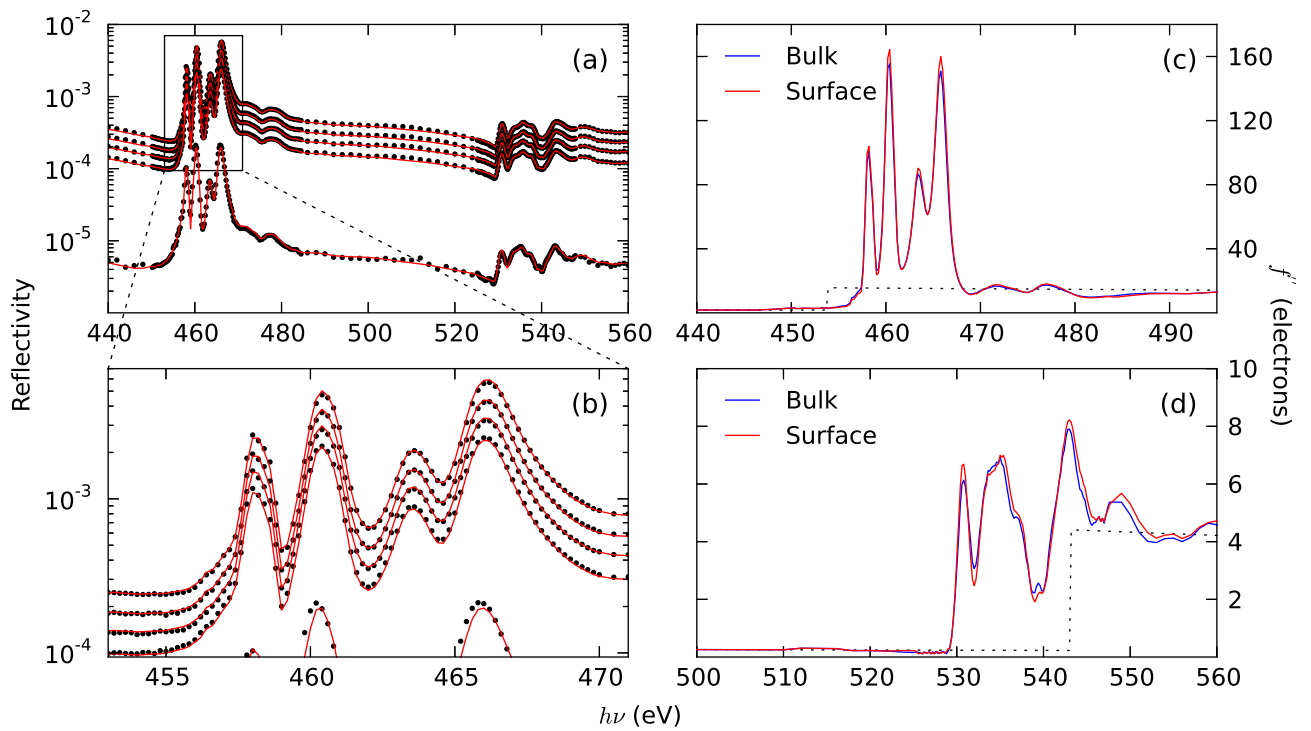


TABLE I. Refinement details for each of the models considered. Those parameter values marked with an * were held fixed during refinement.

	Model #1	Model #2	Model #3a	Model #3b
Surface Layer Thickness (\AA)	-	4.933	9.539	9.622
Surface Layer Roughness (\AA)	-	3.296	3.928	3.477
Surface Layer Density (g/cm^3)	-	1.674	1.057	1.073
Surface Layer Composition	-	C*	C*	C*
STO Surface Layer Thickness (\AA)	-	-	21.653	21.242
STO Surface Layer Roughness (\AA)	-	-	2.727	2.424
STO Surface Layer Density (g/cm^3)	-	-	5.13*	5.13*
STO Surface Layer Composition	-	-	$\text{Sr}_{1.252}\text{Ti}_1\text{O}_{3.252}$	$\text{Sr}_{1.238}\text{Ti}_1\text{O}_{3.238}$
STO Bulk Layer Thickness (\AA)	∞^*	∞^*	∞^*	∞^*
STO Bulk Layer Roughness (\AA)	10.603	5.423	9.346	6.745
STO Bulk Layer Density (g/cm^3)	5.13*	5.13*	5.13*	5.13*
STO Bulk Layer Composition	SrTiO_3^*	SrTiO_3^*	SrTiO_3^*	SrTiO_3^*
Figure of Merit $\left(\sum \left[\frac{Y_{\text{obs}} - Y_{\text{calc}}}{Y_{\text{obs}}} \right]^2 \right)$	0.0368	3.258	5.344	3.518
Number of Parameters	221	302	307	607
Number of Data Points	224	1356	1695	1695